Rapid Communications

Ordering of sedimenting paramagnetic colloids in a monolayer

Ludovic Spiteri,[1,2] René Messina,[1] David Gonzalez-Rodriguez,[2] and Lydiane Bécu[2,*]
[1]*Laboratoire de Physique et Chimie Théoriques LPCT–UMR CNRS 7019, Université de Lorraine, 1 Boulevard Arago, 57070 Metz, France*
[2]*LCP-A2MC, Institut Jean Barriol, Université de Lorraine, 1 Boulevard Arago, 57070 Metz, France*

(Received 26 February 2018; published 16 August 2018)

Sedimentation enables self-assembly of colloidal particles into crystalline structures, as needed for catalysis or photonics applications. Here we combine experiments, theory, and simulations to investigate the equilibrium structure of a colloidal monolayer with tunable interparticle repulsion via an applied external magnetic field. Experimental observations of the equilibrium structure are in excellent agreement with density functional theory. Within a (zero-temperature) local density approximation, we derive a simple analytical expression that quantitatively captures the inhomogeneous ordering ranging from solid to liquidlike states. Monte Carlo simulations corroborate these findings and explore an even wider range of sedimentation conditions, thus providing a global view of the sedimentation-mediated ordering in colloidal monolayers with tunable long-ranged interparticle repulsions. Our findings shed further light on the classical sedimentation problem in colloidal science and related areas.

DOI: 10.1103/PhysRevE.98.020601

The self-assembly of colloidal particles into crystalline structures has attracted significant attention over the past decades [1–6] (for a review, see [7]). Besides opening the way to many technological applications in various fields including photonics, chemical sensors, and catalysis [8–10], the study of colloidal self-assembly has also provided new insights into the physics of crystallization thanks to the experimentally accessible length, time, and energy scales of colloidal systems [2,11–14]. Sedimentation is commonly used to manufacture colloidal crystals, as it provides a simple way to locally increase the volume fraction of a colloidal suspension to induce crystallization.

Since the seminal work by Perrin [15], sedimentation has stimulated a wealth of statistical mechanics studies of complex fluids under gravity [16–26] (for a review, see [27]). Measuring the equilibrium density profile of colloidal suspensions provides a method to characterize the thermodynamical properties of the system [17,18]. The classical density functional theory (DFT) constitutes a well-known tool to describe the equilibrium density profiles for different interparticle interactions, including hard spheres or screened Coulomb [17,19,20], electrostatic [18,21] or magnetic [22] pair potentials, and mixtures of colloids and polymers [23,24].

Recently, crystallization in a tilted monolayer was studied for a system of hard spheres, allowing a full description of the phase diagram of two-dimensional hard-sphere colloids [25]. On the other hand, sedimentation experiments of a ferrofluid have been conducted recently in a three-dimensional system and successfully fitted by a perturbed virial expansion approach [26]. In this Rapid Communication, we propose an original experiment where the sedimentation of a two-dimensional array of paramagnetic colloids, whose interaction potential can be controlled by an external magnetic field, is visualized through optical microscopy. In conjunction, we derive a DFT model and develop numerical simulations to further outline the physics of sedimented paramagnetic colloids in two dimensions.

A suspension of superparamagnetic particles (Dynabeads M-450, diameter $2R = 4.4\ \mu$m; Life Technologies) is allowed to sediment to the bottom of a rectangular quartz cuvette (Hellma Analytics), forming a 1 cm $\times$ 1 cm bidimensional array of average initial density ρ_i. A coil of diameter 13 cm and height 2.5 cm with 95 loops is centered around the cuvette to generate a magnetic field B_z perpendicular to the array, inducing a repulsive magnetic potential between neighboring colloids. The coil and cuvette rest on a plate that can be tilted to a chosen angle α with respect to the horizontal, subjecting the particles to an in-plane gravity component, $g \sin\alpha$, which drives particle sedimentation along the y direction [see Fig. 1(a) for a sketch of the setup]. The whole setup is built on the stage of an inverted microscope equipped with a CCD camera. It is thus possible to translate the setup along the y direction in order to access the full density profile of the colloidal array. Due to the small angle existing between the sample plane and the imaging plane, the imaging plane needs to be refocused during stage translation, whereas focus differences within one image are negligible. A typical experimental snapshot reconstructed from images recorded along the y direction is presented in Fig. 1(b). A dense ordered sediment is observed at the lowermost edge of the plane bottom around $y = 0$. In this region, the sediment exhibits a polycrystalline microstructure, characterized by localized crystallites with a triangular lattice [Fig. 1(c)] [13]. Upon increasing y, the ordering decreases [Fig. 1(b)].

To quantify the ordering of the colloidal suspension, we investigate the spatial variation of the density profile, $\rho(y)$. The latter is defined as the laterally integrated density profile that reads

$$\rho(y) = \frac{1}{L_x}\int_0^{L_x} n(x,y)dx, \tag{1}$$

*lydiane.becu@univ-lorraine.fr

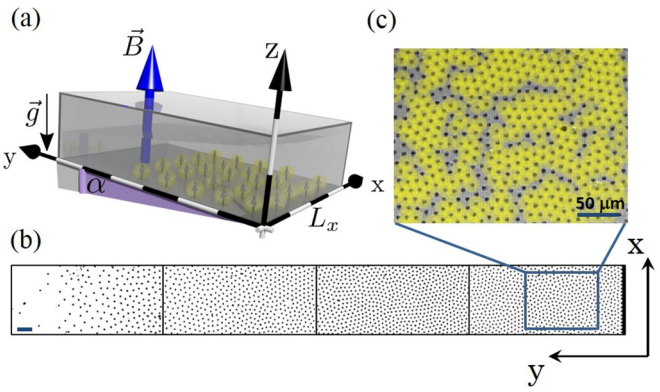

FIG. 1. Sedimentation of a two-dimensional monolayer of paramagnetic colloids. (a) Sketch of the experimental setup allowing a layer of colloids confined in the (x, y) plane to be tilted by an angle α to drive sedimentation along the y direction. (b) Experimental sedimentation profile reconstructed from snapshots recorded at different positions y for a tilt angle $\alpha = 1.6^\circ$ at $B = 0.9$ mT. A threshold has been applied to the images for better visibility. The scale bar corresponds to 50 μm. (c) Details of a typical experimental image. Particles arranged on a triangular lattice are surrounded by six neighbors and are highlighted in yellow.

where $n(x, y)$ stands for the local particle density on the (x, y) plane and L_x is the bottom edge [see also Fig. 1(b)]. We analytically describe $\rho(y)$ by a DFT approach that we briefly describe in what follows. The pair potential of two parallel identical magnetic dipoles of magnitude χB is $U_{ij}^{(\mathrm{dip})} = \frac{\mu_0}{4\pi}\frac{\chi^2 B^2}{r_{ij}^3}$, where μ_0 is the permeability, χ is the magnetic susceptibility, and r_{ij} is the distance between the two dipolar particles i and j. At prescribed coordinate y, it is assumed that the local density $\rho(y)$ results from a triangular lattice with lattice constant $a(y)$ yielding $\rho(y) = 2/[\sqrt{3}a(y)^2]$. Thereby, the dipole potential energy associated with particle i located at y_i obeys $U_i^{(\mathrm{dip})} = \frac{1}{2}\sum_j U_{ij}^{(\mathrm{dip})} = \frac{2M}{5}\frac{\mu_0}{4\pi}\chi^2 B^2 \rho(y_i)^{3/2}$ where $M = 2^{-7/2}3^{3/4}5M_0 \approx 11.116$ is a geometrical constant with $M_0 \approx 11.034$ denoting the Madelung constant obtained by lattice sum [28,29]. The gravity contribution is merely given by $U_i^{(\mathrm{gravity})} = mgy_i \sin\alpha$, so that the total potential energy associated with particle i at y_i reads $U_i = U_i^{(\mathrm{gravity})} + U_i^{(\mathrm{dip})}$. Within this framework, we are able to write the free energy of the system per unit width L_x (see also the setup in Fig. 1) as [17]

$$\beta F = \int_0^\infty \left(\rho(y)\{[\ln(\Lambda^2\rho(y))] - 1\} + \rho(y)\frac{y}{\ell_s} + \frac{2M}{5}\Gamma\ell_s^3\rho(y)^{5/2}\right)dy, \tag{2}$$

where Λ is the (irrelevant) thermal wavelength, and m is the effective mass of a particle (corrected for buoyancy). The first term in Eq. (2) represents the ideal gas part. The second term is the gravity contribution with $\ell_s = (\beta mg \sin\alpha)^{-1}$ denoting the sedimentation length, where $\beta = 1/k_BT$ (k_B is the Boltzmann constant and T the temperature). The last term corresponds to the dipole-dipole interaction with $\Gamma \equiv \frac{\mu_0}{4\pi}\frac{\chi^2 B^2}{k_B T \ell_s^3}$ being the dimensionless magnetic coupling. At equilibrium, the free energy is minimum, subjected to the condition of conservation of the total number of particles, i.e., $\int_0^\infty \rho(y)dy = \rho_x$, where ρ_x is the projected density, obtained as the number of particles divided by L_x. Denoting $\rho_0 = \rho(y = 0)$, the resulting Euler-Lagrange equation related to Eq. (2) can be written as

$$\ln\frac{\rho(y)}{\rho_0} + M\Gamma\left[\rho(y)^{3/2} - \rho_0^{3/2}\right]\ell_s^3 = -\frac{y}{\ell_s} \tag{3}$$

with $\rho_0 = \rho_0(\rho_x)$. At this stage, static quantities are fully determined by assigning values to Γ and ρ_x and employing ℓ_s as unity of length. In the high-temperature limit $\Gamma\rho_x^3\ell_s^3 \ll 1$, the logarithmic term in Eq. (3) dominates and the well-known Perrin's result $\rho(y) = \frac{\rho_x}{\ell_s}\exp(-y/\ell_s)$ is recovered [15]. Interestingly, in the low-temperature limit $\Gamma\rho_x^3\ell_s^3 \gg 1$, the logarithmic term in Eq. (3) becomes negligible. In that regime, the following relevant result is obtained:

$$\left(\frac{\rho(y)}{\rho_0}\right)^{3/2} = 1 - \frac{y}{y_{\max}}, \tag{4}$$

where $\rho_0 = (5/3)^{2/5}\gamma^{2/5}\rho_x^2$ and $y_{\max} = (5/3)^{3/5}\gamma^{-2/5}\rho_x^{-1}$ with $\gamma = (\Gamma\rho_x^4\ell_s^4 M)^{-1} = \frac{4\pi mg\sin\alpha}{M\mu_0\chi^2B^2\rho_x^4}$ reflecting the ratio between the gravity potential and the magnetic interaction. Equation (4) will be referred to as the zero-temperature local density approximation (LDA) result (or model). In what follows, this remarkably simple analytical expression (4) will be tested against experiments and simulations.

To gain further insight into the physical mechanisms of sedimenting paramagnetic colloids in two dimensions, Monte Carlo (MC) simulations based on the (exact) Hamiltonian, $\beta U_{\mathrm{MC}} = \sum_i \frac{y_i}{\ell_s} + \frac{1}{2}\sum_{i\neq j}\frac{\Gamma\ell_s^3}{r_{ij}^3}$, are performed in the canonical ensemble mimicking the experimental situation. The number of particles N is fixed at $N = 1000$ [30]. The simulation cell consists of a $L_x \times L_y$ rectangular box with periodicity in the x direction, consistent with the setup in Fig. 1. The long-range dipole-dipole interactions are computed using a Lekner-like sum technique adapted for systems with periodicity in one direction [31]. Typically 10^5–10^6 MC steps are devoted for equilibration and statistics are gathered over an additional 10^6 MC steps.

The experimental density profiles normalized according to the zero-temperature LDA model [see Eq. (4)] are displayed in Figs. 2(a) and 2(b) [32]. We adopt as our baseline conditions $\alpha = 2^\circ$ and $B = 0.9$ mT, corresponding to $\gamma \approx 3.0 \times 10^{-4}$ [33]. Figure 2 shows the effect (a) of varying the strength of the magnetic field and (b) of changing the slope. In both cases, an excellent agreement between theory and experiment is found. Figures 2(d)–2(f) show experimental snapshots for $\alpha = 2^\circ$ and different strengths of the magnetic field. A similar structural evolution is observed upon increasing the slope at constant magnetic field. In the same spirit as the experiments, we also choose a reference system in our simulations ($\Gamma = 100$, $g^* = 1$) defining the reference sedimentation length $\ell_s^{(\mathrm{ref})}$ [34]. The corresponding density profile is displayed in Fig. 3(b). A smoothing of the simulation density profiles [35] covering a wide range of Γ and g^* values (see Fig. 3), leads to a virtually quantitative agreement with theory [see Fig. 2(c)]. Hence, the experimental profiles exhibit an identical behavior to that of the smoothed density profiles stemming from the MC

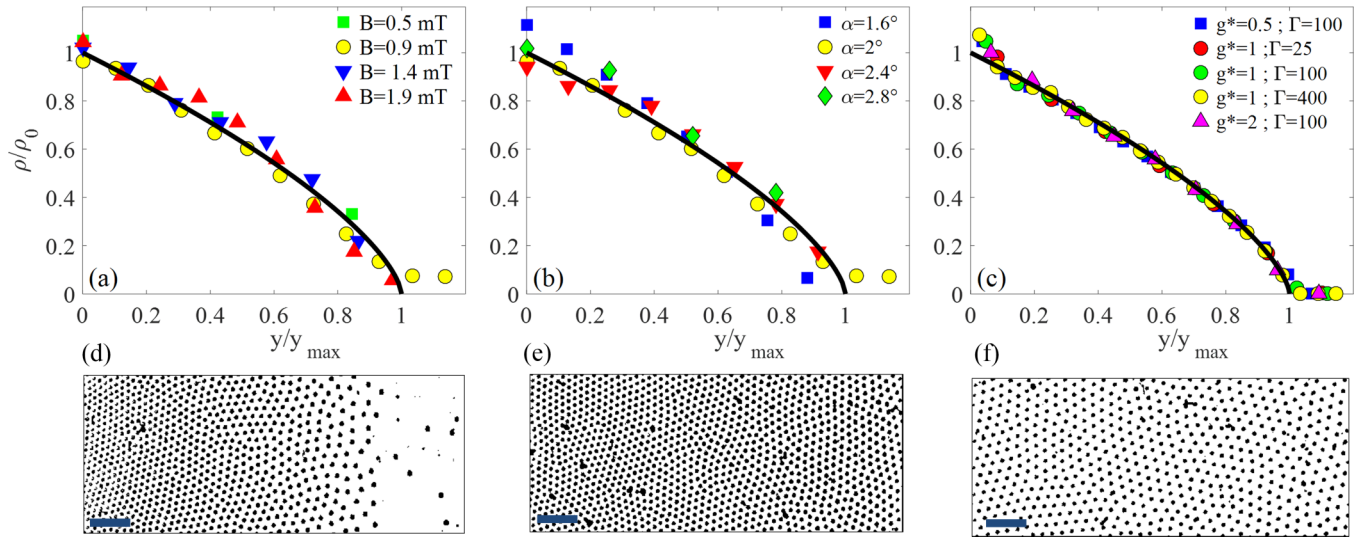

FIG. 2. Density profiles normalized according to the theoretical model as a function of the normalized upslope distance [see Eq. (4) and definitions of $y_{\max}$ and ρ_0 in the text]. The black line in each plot is the theoretical prediction given by Eq. (4). Experimental profiles (a) for different values of the magnetic field B at fixed inclination angle $\alpha = 2^\circ$ and (b) for different values of α at constant magnetic field $B = 0.9$ mT. (c) Simulation profiles for different values of g^* and Γ. Experimental snapshots of the sedimented monolayer recorded at $y = 490-980$ μm are shown for $\alpha = 2^\circ$ and $B = 0.5$ mT (d), $B = 0.9$ mT (e), and $B = 1.9$ mT (f). The scale bars correspond to 50 μm.

simulations. The absence of oscillations in the experiments is due to polycrystallinity, detectable in Fig. 1(c), which averages out the density oscillations of single domains.

The vivid *oscillatory* behavior revealed in the bare simulation density profiles is a signature of the strong layering occurring around the bottom edge (see Fig. 3) [17,19]. Sufficiently

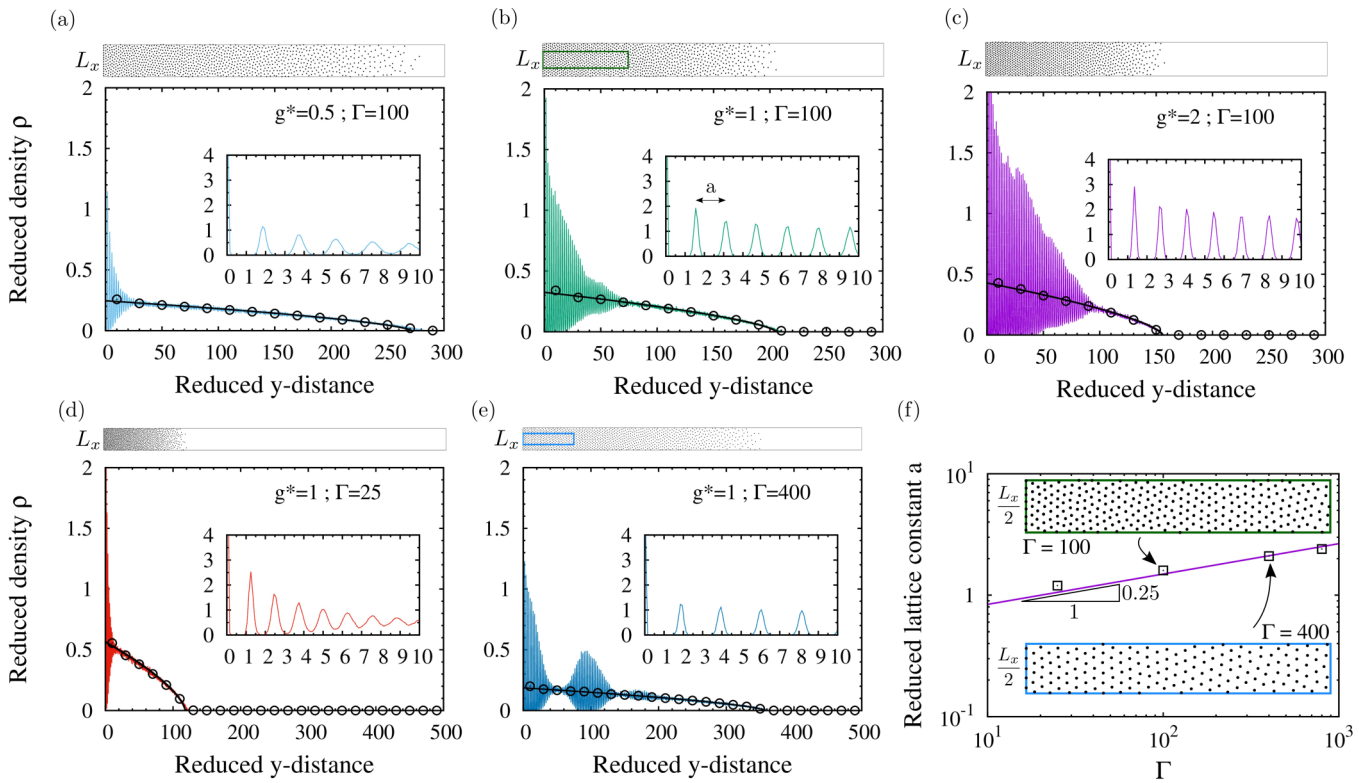

FIG. 3. Monte Carlo simulation density profiles with magnetic coupling $\Gamma = 100$ for different values of the gravity parameter (a) $g^* = 0.5$, (b) $g^* = 1$, and (c) $g^* = 2$. Two additional profiles at prescribed $g^* = 1$ with (d) $\Gamma = 25$ and (e) $\Gamma = 400$ are also displayed. The thick (black) line is the LDA theoretical prediction [see Eq. (4)]. The circles represent the smoothed density profiles (see also text). The insets show a magnified view. Accompanying microstructure snapshots are sketched on the top of panels (a)–(e). (f) Lattice constant a; see inset of (b) of for illustration, as a function of Γ with $g^* = 1$. The solid line is the best fit for a power law of the form $\Gamma^{0.25}$. The insets are a magnified view of the boxed regions in snapshots shown in (b) and (e). The unit length is $\ell_s^{(\mathrm{ref})}$ for the whole figure.

far away from the bottom edge, nonsmoothed profiles quantitatively match with theory, signaling a disordered state (see also snapshots provided in Fig. 3). Increasing gravity alone at prescribed magnetic field ($\Gamma = 100$) enhances the ordering and its range [see Figs. 3(a)–3(c). Concomitantly, the (apparent) lattice constant a [distance between two successive peaks; see inset in Fig. 3(a)] decreases with gravity. Upon increasing the magnetic field at prescribed gravity ($g^* = 1$) [see Figs. 3(b), 3(d) and 3(e)], the range of the layering becomes broader. Thereby, the lattice constant increases with Γ (see Fig. 3). More specifically, a remarkable power law like $a/\ell_s \sim \Gamma^{1/4}$ emerges [ee Fig. 3(c)]. The latter can be rationalized with the simple idea of a balance between gravity force ($\sim g = \text{const}$) and repulsive magnetic force ($\sim \Gamma/a^4$). Interestingly, at strong coupling $\Gamma = 400$ [see Fig. 3(e)], the density profile is reminiscent of a standing wave as a result of a nontrivial balance between gravity (pushing the particles toward the bottom) and strong repulsive magnetic interaction (expelling particles from the bottom). In the situation of moderate layering with $\Gamma = 25$ [see Fig. 3(d)], it is worth mentioning that the simple zero-temperature LDA prediction remains robust to describe the smoothed density profile. Thereby, even at a finite temperature well above zero, the zero-temperature LDA approach remains suited to characterize density profiles far from strong ordering.

In summary, we have experimentally and theoretically advocated the ordering mediated by a nontrivial balance between sedimentation and long-ranged dipole-dipole interparticle repulsion occurring within a colloidal monolayer. The experimental density profiles are in excellent agreement with predictions from density functional theory and Monte Carlo simulations. Thereby, a strikingly simple analytical solution, based on the zero-temperature limit in the local density approach, has been derived [see Eq. (4)]. The latter accounts for the experimentally found density profiles ranging from the solidlike state (close to the bottom edge) to the liquidlike state (far from the bottom edge). Computer simulations indicate that strong crystal layering occurs, near the container's bottom wall, as signaled by vivid oscillations in density profiles. The associated lattice constant is roughly dictated by $\Gamma^{1/4}$, reflecting merely a force balance between gravity and dipole-dipole interaction. Such oscillations are smoothed out in experiments, an effect attributed to polycrystallinity. It would be interesting for future studies to check whether our approach can be generalized to other soft repulsive potentials such as a power law of the interparticle distance [36] or a screened Coulomb potential. Overall, our findings demonstrate that the microstructure of the sediment can be tuned and predicted by choosing the sedimentation slope and the external magnetic field, thus providing an efficient and convenient technique for the fabrication of controlled ordered monolayers.

This work has been partially funded by the European Union through the program FEDER-FSE Lorraine et Massif des Vosges 2014-2020.

[1] P. N. Pusey and W. van Megen, Nature (London) **320**, 340 (1986).
[2] K. Zahn, R. Lenke, and G. Maret, Phys. Rev. Lett. **82**, 2721 (1999).
[3] K. Zahn and G. Maret, Phys. Rev. Lett. **85**, 3656 (2000).
[4] U. Gasser, E. R. Weeks, A. Schofield, P. N. Pusey, and D. A. Weitz, Science **292**, 258 (2001).
[5] J. P. Hoogenboom, D. Derks, P. Vergeer, and A. van Blaaderen, J. Chem. Phys. **117**, 11320 (2002).
[6] A. Merlin, J.-B. Salmon, and J. Leng, Soft Matter **8**, 3526 (2012).
[7] U. Gasser, J. Phys.: Condens. Matter **21**, 203101 (2009).
[8] J. F. Galisteo-López, M. Ibisate, R. Sapienza, L. S. Froufe-Pérez, Á. Blanco, and C. López, Adv. Mater. **23**, 30 (2011).
[9] J. H. Holtz and S. A. Asher, Nature (London) **389**, 829 (1997).
[10] O. D. Velev and E. W. Kaler, Adv. Mater. **12**, 531 (2000).
[11] P. N. Pusey, W. van Megen, S. M. Underwood, P. Bartlett, and R. H. Ottewill, J. Phys.: Condens. Matter **2**, SA373 (1990).
[12] J.-P. Hansen, D. Levesque, and J. Zinn-Justin, *P. N. Pusey in: Liquids, Freezing and the Glass Transition, Les Houches Session LI* (Elsevier, Amsterdam, 1991).
[13] L. Assoud, F. Ebert, P. Keim, R. Messina, G. Maret, and H. Löwen, Phys. Rev. Lett. **102**, 238301 (2009).
[14] R. Messina, S. Aljawhari, L. Bécu, J. Schockmel, G. Lumay, and N. Vandewalle, Sci. Rep. **5**, 10348 (2015).
[15] J. Perrin, J. Phys. Theor. Appl. **9**, 5 (1910).
[16] A. Vrij, J. Chem. Phys. **72**, 3735 (1980).
[17] T. Biben, J.-P. Hansen, and J.-L. Barrat, J. Chem. Phys. **98**, 7330 (1993).
[18] T. Biben and J. P. Hansen, J. Phys.: Condens. Matter **6**, A345 (1994).
[19] T. Biben, R. Ohnesorge, and H. Löwen, Europhys. Lett. **28**, 665 (1994).
[20] C. P. Royall, J. Dzubiella, M. Schmidt, and A. van Blaaderen, Phys. Rev. Lett. **98**, 188304 (2007).
[21] A. Esztermann and H. Löwen, Europhys. Lett. **68**, 120 (2004).
[22] T. Kruppa, T. Neuhaus, R. Messina, and H. Löwen, J. Chem. Phys. **136**, 134106 (2012).
[23] M. Schmidt, M. Dijkstra, and J.-P. Hansen, Phys. Rev. Lett. **93**, 088303 (2004).
[24] M. Schmidt, M. Dijkstra, and J.-P. Hansen, J. Phys.: Condens. Matter **16**, S4185 (2004).
[25] A. L. Thorneywork, J. L. Abbott, D. G. A. L. Aarts, and R. P. A. Dullens, Phys. Rev. Lett. **118**, 158001 (2017).
[26] E. A. Elfimova, A. O. Ivanov, E. V. Lakhtina, A. F. Pshenichnikov, and P. J. Camp, Soft Matter **12**, 4103 (2016).
[27] R. Piazza, Rep. Prog. Phys. **77**, 056602 (2014).
[28] E. Madelung, Phys. Z. **19**, 542 (1918).
[29] M. M. Hurley and S. J. Singer, J. Phys. Chem. **96**, 1938 (1992).
[30] We have performed beforehand some simulations with $N = 2000$. It turns out that the density profiles are virtually undistinguishable from those obtained with with $N = 1000$. Hence we are confident that our two-dimensional systems with $N = 1000$ do not suffer from finite size effects.
[31] A. Grzybowski and A. Brodka, Mol. Phys. **101**, 1079 (2003).
[32] Density profiles $\rho(y)$ are obtained by counting the number of particles located in a window of width $d_y = 100\ \mu$m centered around the coordinate y. When a smaller width is used, the

resulting profiles become very noisy, due to windows becoming smaller than the polycrystal sizes.

[33] The corresponding value of the gravitational length in our experiments, based on a temperature $T \approx 300$ K and a particle buoyant weight $mg \approx 2.210^{-13}$ N, is $l_s \approx 1$ μm.

[34] In order to establish a tractable comparison between experiments and simulations, we introduce a reduced effective gravity $g^* \equiv \frac{g_{\rm eff}}{g_{\rm ref}}$ where $g_{\rm eff} = g \sin\alpha$ and $g_{\rm ref} = g \sin\alpha_{\rm ref}$. For the reference case, $\ell_s = \ell_s^{(\rm ref)}$ where $g^* = 1$ and $\Gamma = 100$. A rectangular cell with $L_x = 25\ell_s^{(\rm ref)}$ and $L_y = 1000\ell_s^{(\rm ref)}$ has been used for all the presented simulations.

[35] The smoothed density profiles are achieved by coarsening the bin width of bare (oscillating) profiles over typically $20\ell_s^{(\rm ref)}$.

[36] S. C. Kapfer and W. Krauth, Phys. Rev. Lett. **114**, 035702 (2015).